J Nanostruct 15(3): 997-1008, Summer 2025

RESEARCH PAPER

Structural Characterization and Cytotoxicity Evaluation of $Ce_{0.5}Nd_{0.5}O_{1.75}$ Nanostructures as Novel Cancer Therapeutic Agent

Ruaa H.Hassani *, Najwa J. Jubier

Department of Physics, College of Science, University of Wasit, Iraq

ARTICLE INFO

Article History:
Received 12 March 2025
Accepted 24 June 2025
Published 01 July 2025

Keywords:
$Ce_{0.5}Nd_{0.5}O_{1.75}$
Green synthesis
Lung cancer
MTT assay

ABSTRACT

This study determined the surface morphological, structural, and biological properties of the green synthesized $Ce_{0.5}Nd_{0.5}O_{1.75}$ nanostructures with aim of exploration of its potential as a novel therapeutic agent for cancer treatment. Observations showed a well-designed quasi-spherical sample with an average particle size of 38.60 nm. XRD pattern revealed highly crystalline in nature with a cubic crystal structure and a crystallite size of 9.25 nm. EDX analysis showed the elemental composition with atomic percentages of 41.17% for O, 31.69% for Nd, and 27.14% for Ce. Raman spectrum demonstrated a prominent peak at 460 cm^{-1} and a secondary peak at 600 cm^{-1}, indicating the F2g symmetric breathing mode and presence of oxygen vacancies. The biological properties of the samples were studied using the MTT assay to evaluate cytotoxicity against A549 lung cancer cells. Six concentrations (6.25–200 µg/mL) were tested, with significant reductions in cell viability observed at concentrations ≥12.5 µg/mL. The $Ce_{0.5}Nd_{0.5}O_{1.75}$ nanostructures exhibited a dose-dependent cytotoxic profile with an IC50 of approximately 100 µg/mL. Compared to standard chemotherapies like cisplatin and pemetrexed, which induced almost complete cell death at higher doses, the $Ce_{0.5}Nd_{0.5}O_{1.75}$ nanostructures showed a more gradual and potentially less toxic impact on cell viability. Fluorescence imaging corroborated these findings, showing intense fluorescence in control cells and reduced fluorescence in treated cells, indicative of metabolic disruption. Three different treatment conditions demonstrated the nanostructure's potential for targeted therapy with lower toxicity. Overall, $Ce_{0.5}Nd_{0.5}O_{1.75}$ offers promising prospects as a cancer therapeutic agent due to its unique structural attributes and controlled biological interactions.

How to cite this article
Hassani R., Jubier N. Structural Characterization and Cytotoxicity Evaluation of $Ce_{0.5}Nd_{0.5}O_{1.75}$ Nanostructures as Novel Cancer Therapeutic Agent. J Nanostruct, 2025; 15(3):997-1008. DOI: 10.22052/JNS.2025.03.017

INTRODUCTION

Rare earth elements are an excellent source of new materials because of their unique optical, electrical, and magnetic properties, which stem from their unusual electronic configuration. This article provides an introduction to rare earth composites, along with a review of their synthesis methods and applications across various industries. It also discusses nano-rare earth oxide composites, like $Ce_{0.5}Nd_{0.5}O_{1.75}$ [1]. Oxide materials have fascinated researchers in many fields including medicine, energy, technological advancements, waste management, and environmental studies [2, 3]. Rare earth oxides

* *Corresponding Author Email: ruaah224@uowasit.edu.iq*

(REOs) have many applications across biological, sensor, electrical, optical, and other fields. Recent advancements in the synthesis techniques have demonstrated the versatility of nano-REOs in various forms [4]. Beyond their current uses, some nano-REOs have shown exciting properties that lead to new applications in the future. An objective evaluation includes a discussion of the limitations, problems, and health issues related to the topic. Protein-nanoparticle interaction substantially impacts in vivo biocompatibility and toxicity. In this process, proteins bind to nanoparticles, enabling their entry into cells through receptor-mediated endocytosis, which can lead to cytotoxicity. Furthermore, unsuccessful tagging and genotoxicity can occasionally occur due to non-specific interactions that cause nanoparticles to adhere to cell membranes, the extracellular matrix, and cell nuclei. The biological performance of nanoparticles as toxicity agent is significantly influenced by their size, shape, surface charge, and solubility [5]. Tetrazolium salts have been extensively used in several experimental methods over the years. Their uses include quantifying oxidoreductase activity, identifying the subcellular location of oxidoreductases, detecting superoxide radicals, screening for Mycoplasma, and, most critically, evaluating microbial survival and growth. In the late 20th century and early 21st century, novel procedures were developed that use the reduction process of tetrazolium salts. The synthesis of new compounds in this category, together with our expanding comprehension of the processes behind the reduction of tetrazolium salts, has markedly expedited research in this domain [6]. Most of the chemical reactants employed in bioassays are tetrazolium salt derivatives, particularly the 3-(4, 5-dimethylthiazol-yl)-2, 5-diphenyl tetrazolium bromide (MTT). MTT can be used on fungi, bacteria, and even mammalian cell lines. It is important to note that almost every component of the assay settings varies significantly among the reported procedures. This inconsistency is particularly noteworthy when optimizing a novel set of tests is required [7]. In this research, two types of chemotherapy treatment—cisplatin and pemetrexed— were used as a standard to evaluate the experimental work. Chemotherapy has been commonly acknowledged as therapeutic approach in the treatment of lung cancer. It is considered as most promising strategy for the ultimate control of lung cancer, as radiotherapy and surgery often do not provide a cure, especially in advanced stages of the disease [8, 9].

MATERIALS AND METHODS

This study utilizes salts of rare earth elements to prepare a $Ce_{0.5}Nd_{0.5}O_{1.75}$ sample. The salts included (cerium (III) chloride heptahydrate) and (neodymium chloride hexahydrate), which were added in equal proportion to the distilled water, and the solution was mixed for 15 min. Following this, the plant extract was added, and the pH value of the solution was adjusted accordingly. The mixture underwent centrifugation three times to separate the precipitate, which was then dried

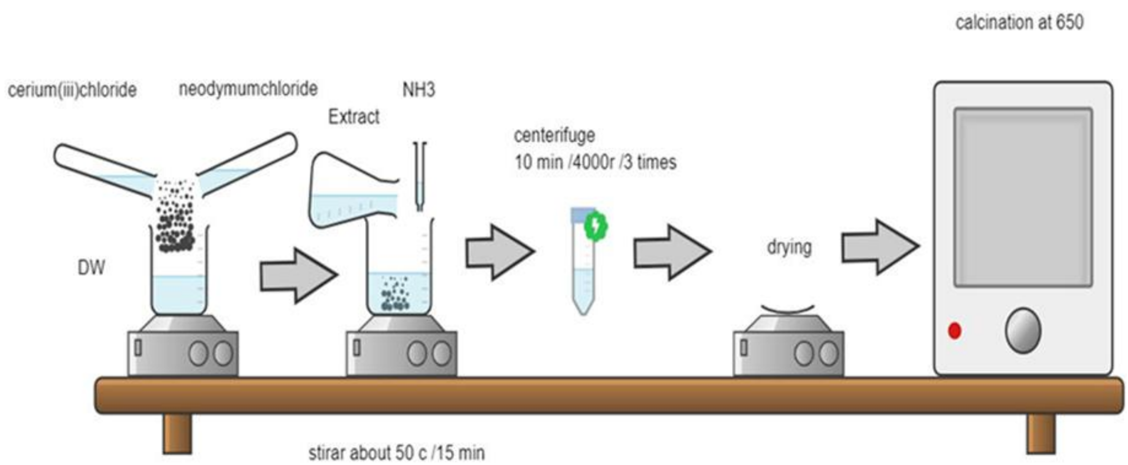

Fig. 1. Schematic diagram of green synthesized $Ce_{0.5}Nd_{0.5}O_{1.75}$ sample.

at 50 °C. After drying, the precipitate was ground and annealed at 600 °C. Composition tests were performed to ensure the purity of the prepared REO nanostructures. The experimental procedure is illustrated in Fig. 1.

RESULTS AND DISCUSSION

XRD data

The crystal structure and phase purity of resulting $Ce_{0.5}Nd_{0.5}O_{1.75}$ were investigated using XRD (Rigaku, Japan) with a Cu-Kα radiation source (λ = 1.5406 Å) in the 2θ range from 10° to 90°. The average crystallite size was determined using Scherrer's formula equal to 9.25 nm [10, 11]. As shown in the XRD pattern, the $Ce_{0.5}Nd_{0.5}O_{1.75}$ sample displayed distinct diffraction peaks in Fig. 2. The pattern shows several distinct peaks, with Miller indices labeled as (111), (200), (202), (311), (400), (313), and (422) for 28.05°, 32.30°, 46.63°, 55.66°, 67.88°, 76.41°, and 86.79°, respectively. The highest intensity peak appears around 28-30° with Miller index (111) show a significant level of structural symmetry across extended distances [12]. The synthesis methodology of the nanocomposite was confirmed to be efficient in developing highly ordered materials. In XRD pattern, sharp, intense peaks were observed, which confirmed that the sample was highly crystalline in nature. From the diffraction pattern, it was established that the sample had a cubic crystal structure. Single phase and no trace of impurity is observed in the material, and the pattern matches with JCPDS data file no. 96-154-1467 [12]. This structural purity points favorable synthesis conditions and evidence of phase development [13].

Morphology

FESEM characterization of the $Ce_{0.5}Nd_{0.5}O_{1.75}$ samples was conducted at various magnifications to examine its morphological features. Fig. 3 shows fundamental characteristics of the synthesized material, describing quasi-spherical nanoparticles with a uniform size distribution averaging 38.60 nm. The nanostructure exhibits distinctive degrees of agglomeration and surface topology of mixed oxide systems. The observed agglomeration can be attributed to two primary factors: Van der Waals forces and surface energy minimization following the Gibbs-Thomson effect. The formation mechanism is evidenced by controlled nucleation and growth kinetics during synthesis, with Ostwald ripening playing a significant role in determining the final particle size distribution [14, 15]. The detailed examination include visible interfaces, neck formation between particles, and evidence of initial stage sintering [16]. The structural characteristics of the $Ce_{0.5}Nd_{0.5}O_{1.75}$ samples such as uniform particle distribution and controlled size range create optimal conditions

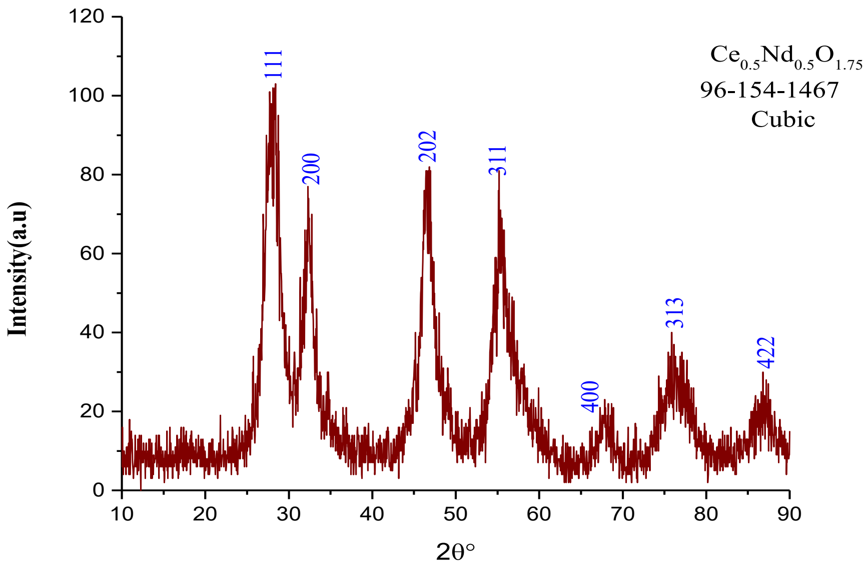

Fig. 2. XRD pattern of green synthesized $Ce_{0.5}Nd_{0.5}O_{1.75}$ nanostructures.

for quantum confinement effects and enhanced surface-dependent properties. This nanoscale integration, combined with the observed interface characteristics, indicates the successful synthesis of a well-integrated system. These structural features are particularly significant for potential catalytic applications, where modified electronic properties and enhanced surface activity are crucial performance parameters [17].

EDX analysis

EDX measurement was utilized to determine the atomic, weight, and error percentage of the existing elements. It provides an overall line of the sample by studying near-surface elements and estimating the elemental proportion at various

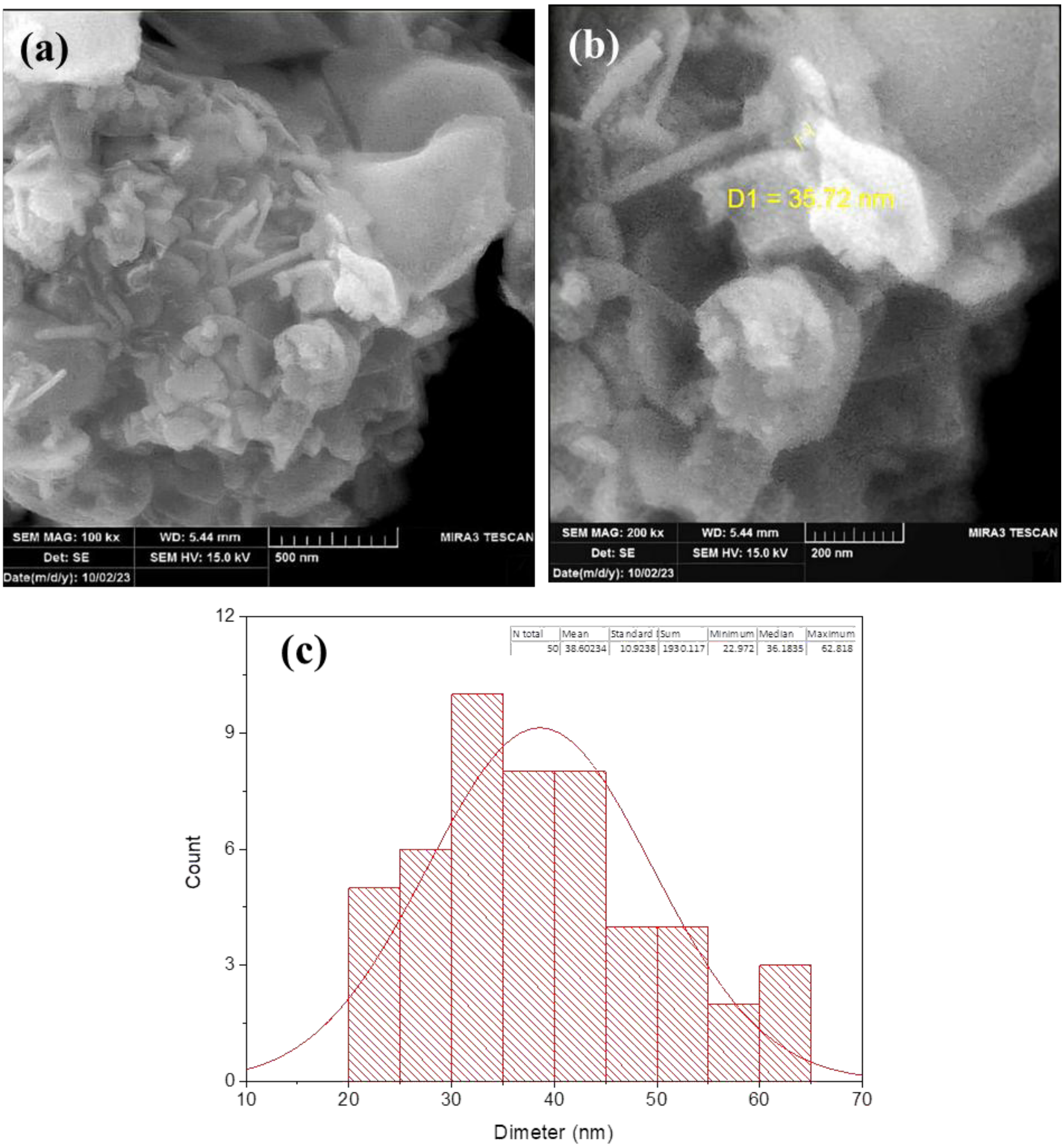

Fig. 3. (a, b) FESEM images and (c) particle size distribution histogram of resulting $Ce_{0.5}Nd_{0.5}O_{1.75}$ samples.

sites [18, 19]. EDX analysis was conducted on the $Ce_{0.5}Nd_{0.5}O_{1.75}$ samples to investigate its elemental composition and structural characteristics [20]. The EDX spectrum in Fig. 4 revealed distinctive peaks corresponding to Cerium L-series (~4.8-5.0 keV), Neodymium L-series (~0.8-1.0 keV), and Oxygen K-series (~0.5 keV), confirming the presence of all expected elements [21]. The spectrum demonstrated excellent resolution over the 0-10 keV range with a high signal-to-noise ratio and minimal background interference, indicating optimal data collection parameters [22]. Strong peak intensities for Ce and Nd confirmed their significant presence. The well-calibrated energy scale, distinct peak separation, and low background counts validated proper sample preparation techniques and enabled reliable quantitative analysis [23]. The absence of unexpected elemental peaks, minimal baseline noise, and correlation of peak positions with theoretical values indicated high purity with low contamination levels. This analysis demonstrated the successful synthesis of the $Ce_{0.5}Nd_{0.5}O_{1.75}$ nanostructures with high purity, making it suitable for various applications in materials science and catalysis [24]. EDX data showed that Neodymium element possess weight percentage of 41.17 wt.% and an atomic percentage of 11.60 at.%, followed by Oxygen at 31.69 wt.% with a dominant atomic percentage of 80.52 at.%, while Cerium has the lowest content of 27.14 wt.% with an atomic percentage of 7.88 at.% .

Raman spectroscopy

The Raman spectrum of the $Ce_{0.5}Nd_{0.5}O_{1.75}$ nanostructures is shown in Fig. 5, which provide valuable insights into structural properties. The dominant peak observed at approximately 460 cm^{-1} corresponds to the F2g symmetric breathing mode of the Ce-O8 vibrational unit, characteristic of the fluorite structure of CeO_2 [25]. A secondary peak around 600 cm^{-1} (D band) indicates the presence of oxygen vacancies, which are induced by the incorporation of Nd^{3+} ions into the CeO_2 lattice [20]. The broadening of these peaks, combined with their relative intensity ratios suggests the

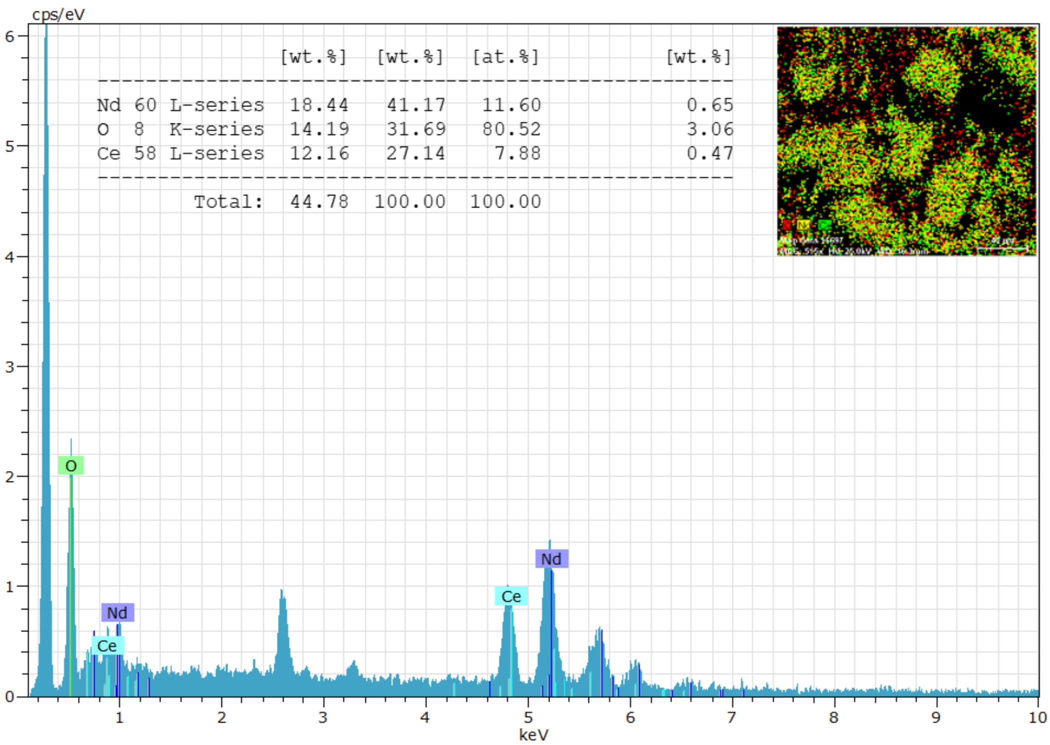

Fig. 4. EDX spectrum of green synthesized $Ce_{0.5}Nd_{0.5}O_{1.75}$ nanostructures.

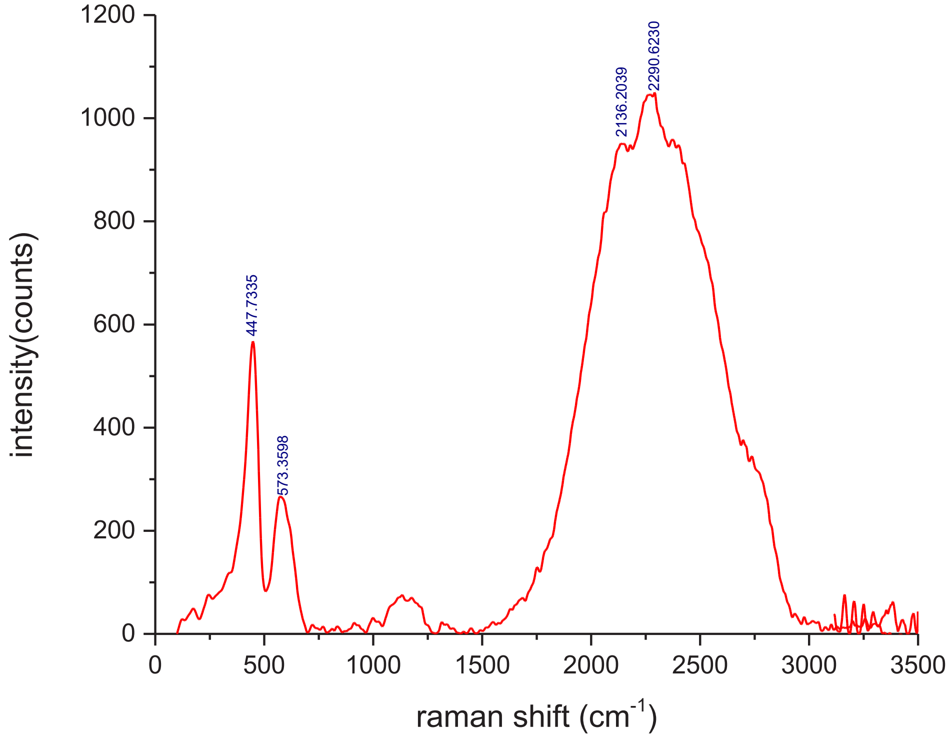

Fig. 5. Raman spectrum of resulting $Ce_{0.5}Nd_{0.5}O_{1.75}$ samples.

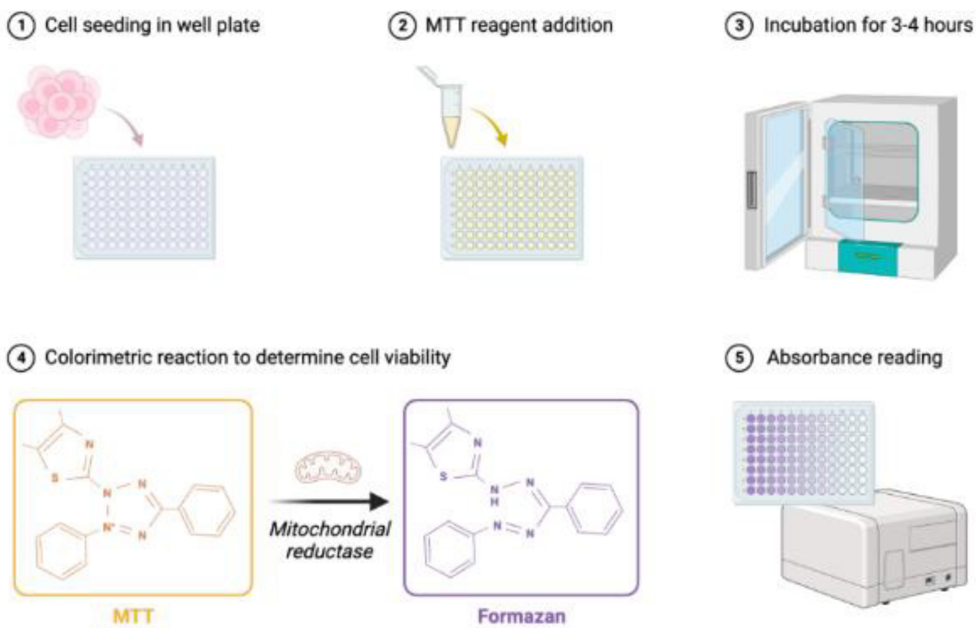

Fig. 6. MTT assay process used in calibrating measures of cell viability.

successful formation of the nanocomposite structure with good crystallinity [26]. The slight shift observed in the F2g mode position, compared to pure CeO_2, provides evidence of effective Nd^{3+} doping, while the presence of additional weak bands in the higher wavenumber region of 2000-2200 cm^{-1} can be attributed to second-order Raman scattering processes [27]. This spectroscopic analysis confirms the successful synthesis of the $Ce_{0.5}Nd_{0.5}O_{1.75}$ nanocompounds and offers valuable information about crystal defects and lattice modifications [28, 29].

Cytotoxicity evaluation

The cytotoxicity tests of the $Ce_{0.5}Nd_{0.5}O_{1.75}$ nanostructures was accomplished by MTT assay using a lung cancer Cell line (A549) within different concentrations ranging from 6.25 to 200 µg/mL. and comparing the results with two types of chemotherapy cancer drugs.

MTT assay principle

MTT assays are generally used to evaluate viable cells in relatively high throughput (96-well plates). Therefore, the common application is assessing the anti-cytotoxicity of a large number of medications at diverse concentrations [30]. The MTT test is predicated on the principle that mitochondrial activity in most viable cells is stable; hence, fluctuations in the number of viable cells correspond directly to changes in mitochondrial activity levels. The synthesis of formazan crystals from the tetrazolium salt MTT give information on the activity of the mitochondria of the cells [31]. Therefore, it becomes possible to count the viable cells by calculating the formazan concentration on the basis of the OD range and notice whether there is an increase or decrease in the number of cells

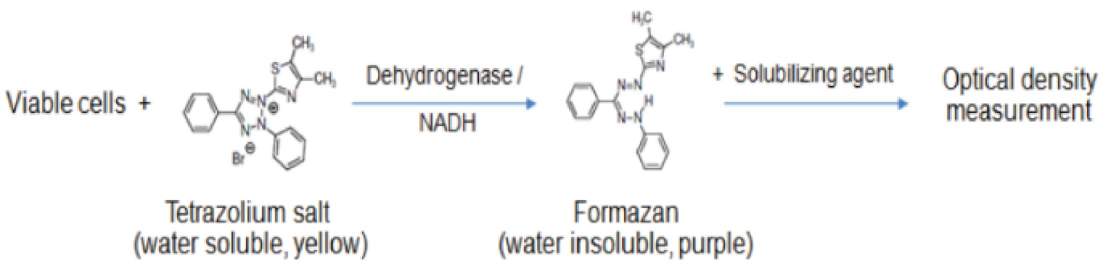

Fig. 7. The mechanism of metabolically active cells in converting yellow tetrazolium to purple formazan crystals [34].

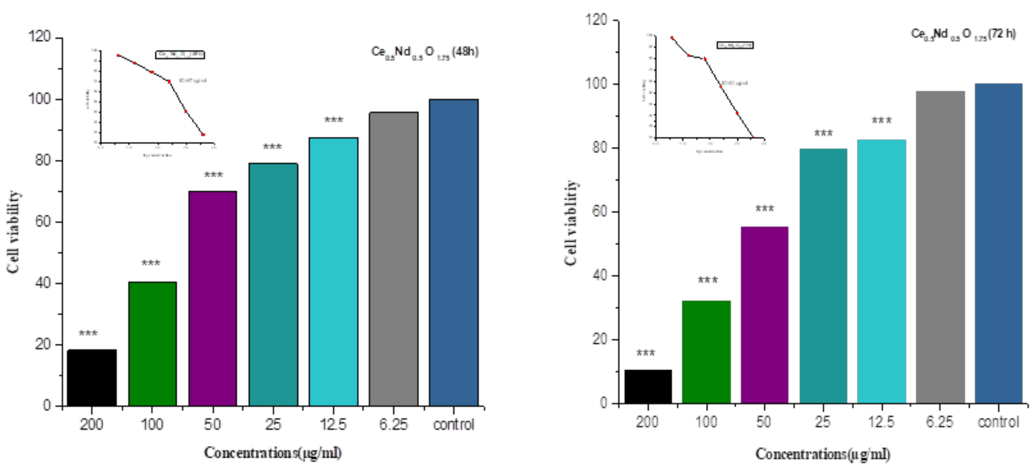

Fig. 8. The plots of cell viability *vs*. the concentration with the IC value for $Ce_{0.5}Nd_{0.5}O_{1.75}$.

[32]. The MTT test may be used to evaluate drug sensitivity in both primary cells and established cell lines. Drug sensitivity measurements differ between cell types in biomedical research. When studying proliferating cell lines, researchers determine the IC50 - the drug concentration that cuts cell growth in half as compared to untreated cells. This work show reduced number cells when their growth is blocked. However, for primary cells that don't normally divide, we look instead at cell death rates. Here, the LC50 tells us what drug concentration kills 50% more cells than would naturally die without treatment. This dual approach helps to understand how drugs affect both growing and stable cell populations in the body.[33]. Fig. 6 shows the MTT assay steps and Fig. 7 illustrates the formation of formazan crystals from the tetrazolium salt MTT.

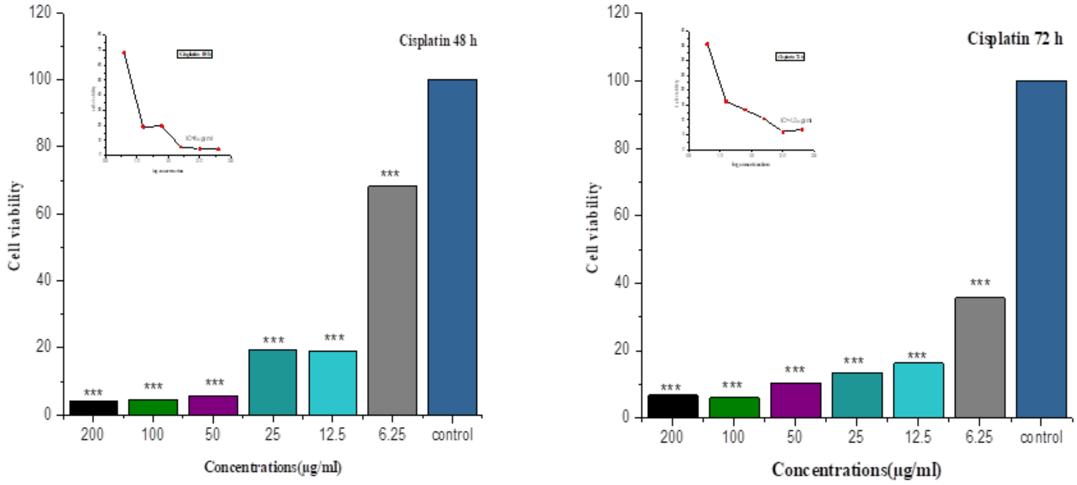

Fig. 9. The plots of cell viability *vs*. the concentration with the IC value for cisplatin chemotherapy.

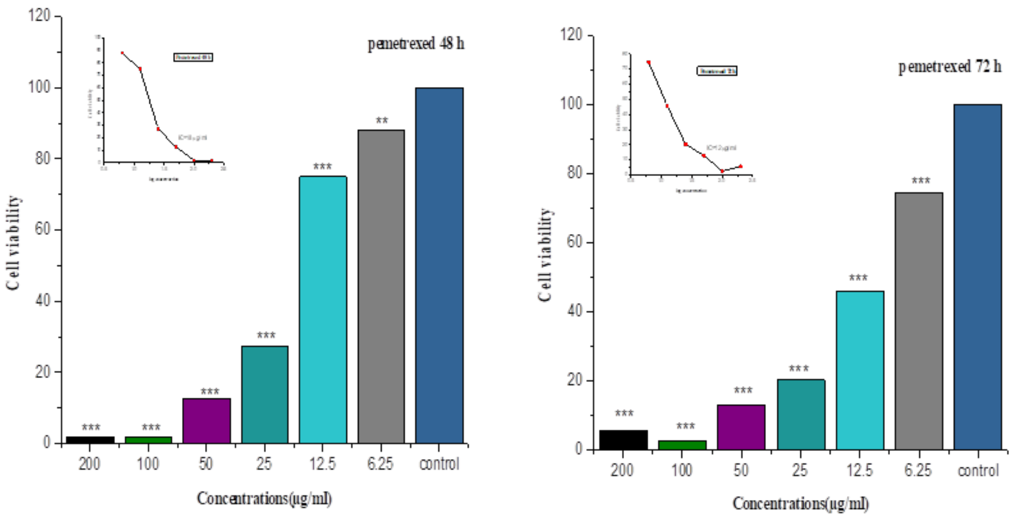

Fig. 10. The plots of cell viability *vs*. the concentration with the IC value for pemetrexed chemotherapy.

Chemotherapy drugs and cell line

Cancer is a disease in which certain body cells proliferate uncontrollably and spread to other parts of the body. Lung cancer is one of the most common diseases in economically developed countries. Due to the population growth and a decline in cleanliness standards, cancer rates are continuously rising, particularly in developed nations [35]. Chemotherapy also known as a chemo is a cancer treatment that involves the uncontrolled growth of damaged abnormal cells [36]. However, these medications can also damage or kill normal healthy cells. Chemotherapy is an effective strategy to prolong the lives of individuals with lung cancer, but a modest survival rate can be achieved due to medication resistance and insufficient bioavailability [37]. Nanomaterials have been investigated as novel delivery systems for cancer treatments, with the most common chemotherapy drugs being cisplatin and pemetrexed. Cisplatin is a platinum chemotherapy used to treat various cancers [38, 39], while pemetrexed disodium is a recently produced antifolate that targets enzymes involved in pyrimidine synthesis [40]. Research on resistance mechanisms in cells with acquired resistance suggests impaired membranes, decreased polyglutamate, elevated enzymes, and structural alterations. Less than 10% of patients with small cell lung cancer survive for more than two years, despite being clinically sensitive to chemotherapy [41]. This study examined the cytotoxic effect of resulting $Ce_{0.5}Nd_{0.5}O_{1.75}$ samples on lung cancer cells by synthesizing them from the rear earth chlorides and plant extract. Cells found on the lining of the bronchi and other lung components, such as the bronchioles or alveoli, may be the first site of lung cancer. As the second most common disease in both men and women, lung cancer is caused to cancer-related deaths [35]. According to previous research, (A549) lung cancer cells and 9 × 10^3 cells/well were incubated for 48 and 72 h at 37 °C in 96-well plates that contained 200 µL of supplemented cell culture medium [30]. Fig.s 8-10 show the cell viability and the concentration of the $Ce_{0.5}Nd_{0.5}O_{1.75}$ samples and the chemotherapy drugs for dual treatments, Statistical analysis was used to investigate quantitative cell viability data. If there was a normal distribution, a one-tailed student's t-test was used to compare the grouped means; p values of less than .001 (***), 001 to .01 (**), and .01 to .05 (*) were deemed significant [42]. This means that there is a 99.9% confidence that the differences between these treatment concentrations (200, 100, 50, 25, and 12.5 µg/mL) and the control group are not due to random chance. You can see that the higher concentrations (200, 100, 50, 25, and 12.5 µg/mL) show these

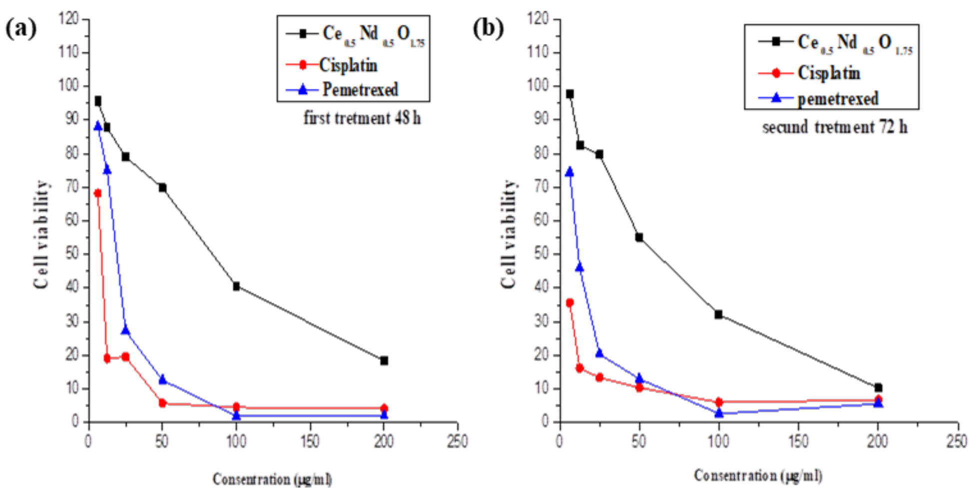

Fig. 11. (a) The cell viability and concentration for the nanocomposite and the chemotherapy drugs during the first treatment at 48 h, (b) the cell viability and concentration for the nanocomposite and the chemotherapy drugs during the first treatment at 72 h.

three stars, indicating they all produced highly significant reductions in cell viability as compared to the control. The absence of stars on the 6.25 μg/mL column suggests that this concentration did not produce a statistically significant difference from the control group.

Fig. 11 records cell viability across different concentrations for 48 h and 72 h. The graph plots include viability (y-axis, ranging from 0-120%) against concentration (x-axis, ranging from 0-250 units). The green synthesized samples and two different types of drugs are compared:" $Ce_{0.5}Nd_{0.5}O_{1.75}$" (black line), "cisplatin" (red line), and "pemetrexed" (blue line). The control point starts at nearly 100% viability for all conditions at zero concentration. As the concentration increases, all three treatments show a declining trend in cell viability, but with different patterns. The black line ($Ce_{0.5}Nd_{0.5}O_{1.75}$) shows a more gradual decrease compared to the other two drugs, maintaining higher viability levels throughout the concentration range and reaching about 20% viability at the highest concentration. In contrast, both "cisplatin" and "pemetrexed" show a much steeper initial decline, dropping to around 20-30% viability in concentration of 50, and then leveling off to nearly 0% viability at higher concentrations. This suggests that "cisplatin" and "pemetrexed" are more potent at reducing cell viability as compared to "$Ce_{0.5}Nd_{0.5}O_{1.75}$" nanostructures. The toxicity analysis of the cell viability graph reveals distinct profiles for the $Ce_{0.5}Nd_{0.5}O_{1.75}$ samples and the drugs tested. The "cisplatin" and "pemetrexed" compounds demonstrate high toxicity levels, reducing cell viability to approximately 20% at relatively low concentrations (around 50 units), with their IC50 values estimated around 40-60 concentration units. In contrast, "$Ce_{0.5}Nd_{0.5}O_{1.75}$" exhibits a notably lower toxicity profile, requiring much higher concentrations to achieve similar cell death rates, with an IC50 of approximately 100 concentration units. The gradual decrease in cell viability suggests a wider therapeutic window for "$Ce_{0.5}Nd_{0.5}O_{1.75}$" compared to the other treatments. "Cisplatin" appears to be the most toxic of all, showing the sharpest initial decline in cell viability, followed closely by "pemetrexed" with a similar high-toxicity profile. The stark difference in toxicity profiles between "$Ce_{0.5}Nd_{0.5}O_{1.75}$" and the other two compounds suggests that while "cisplatin" and " pemetrexed " are more potent, "$Ce_{0.5}Nd_{0.5}O_{1.75}$" might be more suitable for applications where minimal cytotoxicity is crucial [43].

Fluorescence microscopy images of cellular viability are shown in Fig. 12. In a control sample, there is a higher density of bright blue-green fluorescent spots/dots representing viable, metabolically active cells. The difference between

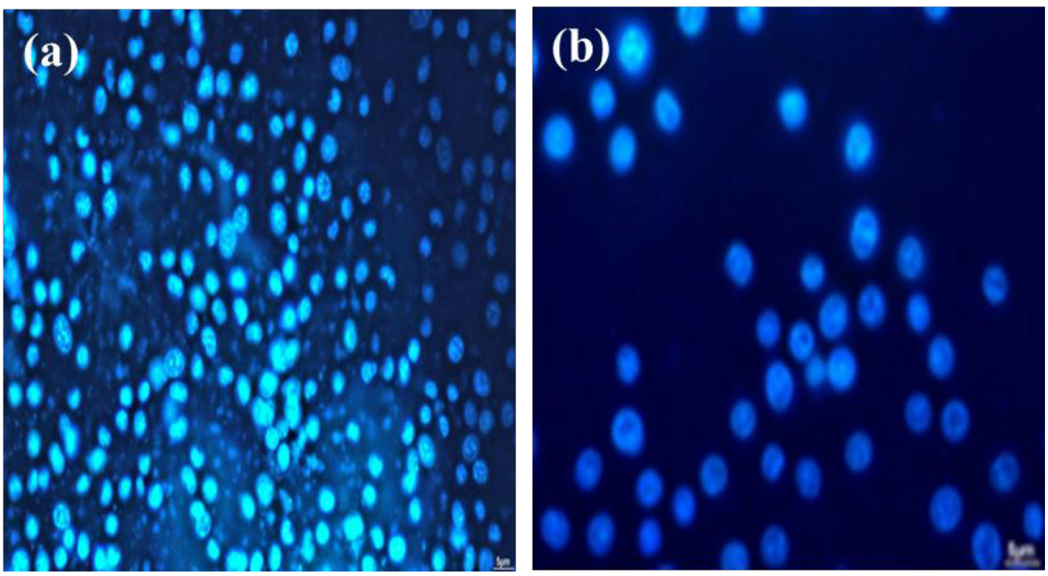

Fig. 12. Florescent images for (a) $Ce_{0.5}Nd_{0.5}O_{1.75}$ and (b) control test.

control and $Ce_{0.5}Nd_{0.5}O_{1.75}$ samples is the overall intensity and distribution of the fluorescent signals. In the control sample, the fluorescent spots are more numerous, brighter, and more evenly distributed across the field of view, indicating a higher level of cellular activity and viability. In contrast, the $Ce_{0.5}Nd_{0.5}O_{1.75}$ samples showed a sparser distribution of fluorescent signals, with darker areas indicating reduced cell viability, likely due to the cytotoxic effects of the treatments being tested. The control sample represents the baseline or normal level of cell viability. By having a control, researchers can determine the cell metabolism and survival treatment effects as compared to the untreated, healthy cells. The comparison between the control and treated samples is crucial for evaluating the cytotoxicity or cytoprotective properties of the compounds in this cell-based assay.

CONCLUSION

Based on the comprehensive study of the $Ce_{0.5}Nd_{0.5}O_{1.75}$, this research presents a significant advancement in cancer therapeutic approaches. The $Ce_{0.5}Nd_{0.5}O_{1.75}$ nanostructures demonstrated remarkable structural characteristics, with a crystallite size of 9.25 nm and a uniform quasi-spherical morphology having an average particle size of 38.60 nm. The cytotoxicity evaluation on A549 lung cancer cell lines revealed a unique cell death profile, with statistically significant cell viability reductions at multiple concentration levels. Notably, the $Ce_{0.5}Nd_{0.5}O_{1.75}$ nanostructures exhibited a more gradual and potentially less toxic reduction in cell viability as compared to traditional chemotherapy drugs like cisplatin and pemetrexed, suggesting a promising alternative in cancer treatment. Diverse analyses, including XRD, FESEM, EDX and Raman spectroscopy confirmed the material's high purity and structural integrity. With controlled cytotoxicity and distinctive biological interactions, the synthesized $Ce_{0.5}Nd_{0.5}O_{1.75}$ nanostructure represents a more targeted and less harmful strategy for cancer therapeutics, which opens new avenues for future research and clinical applications in oncology.

ACKNOWLEDGEMENT

The authors express their gratitude to the Physics Department, University of Wasit, College of Science, for helping us achieve and complete this project.

CONFLICT OF INTEREST

The authors declare that there is no conflict of interests regarding the publication of this manuscript.

REFERENCES

1. Li H, Wei F, Gao R. Application of Nano Rare Earth Materials. E3S Web of Conferences. 2021;257:01026.
2. Lohcharoenkal W, Abbas Z, Rojanasakul Y. Advances in Nanotechnology-Based Biosensing of Immunoregulatory Cytokines. Biosensors. 2021;11(10):364.
3. Vallabani NVS, Singh S. Recent advances and future prospects of iron oxide nanoparticles in biomedicine and diagnostics. 3 Biotech. 2018;8(6):279-279.
4. Hossain MK, Khan MI, El-Denglawey A. A review on biomedical applications, prospects, and challenges of rare earth oxides. Applied Materials Today. 2021;24:101104.
5. Luo D, Cui S, Liu Y, Shi C, Song Q, Qin X, et al. Biocompatibility of Magnetic Resonance Imaging Nanoprobes Improved by Transformable Gadolinium Oxide Nanocoils. Journal of the American Chemical Society. 2018;140(43):14211-14216.
6. Bernas T, Dobrucki JW. The Role of Plasma Membrane in Bioreduction of Two Tetrazolium Salts, MTT, and CTC. Archives of Biochemistry and Biophysics. 2000;380(1):108-116.
7. Young TP, Petersen DA, Clary JJ. The ecology of restoration: historical links, emerging issues and unexplored realms. Ecol Lett. 2005;8(6):662-673.
8. Wood AJJ, Ihde DC. Chemotherapy of Lung Cancer. New England Journal of Medicine. 1992;327(20):1434-1441.
9. Costa SIG, Cauneto VD, Fiorentin-Ferrari LD, Almeida PB, Oliveira RC, Longo E, et al. Synthesis and characterization of Nd(OH)-ZnO composites for application in photocatalysis and disinfection. Chem Eng J. 2020;392:123737.
10. Thamir AA, Jubier NJ, Odah JF. Antimicrobial Activity of Zirconium Oxide Nanoparticles Prepared by the Sol-Gel Method. Journal of Physics: Conference Series. 2021;2114(1):012058.
11. Thamer AA, Jubier NJ, Odah JF. Synthesis and characterization $(ZrO_2$:MgO)Nanocomposite and assessed biocompatibility in vitro by SBF and MTT assay. AIP Conference Proceedings: AIP Publishing; 2024. p. 040009.
12. Vashistha I, Rohilla S. Structural characterization and rietveld refinement of $CeO_2/CoFe_2O_4$ nanocomposites prepared via coprecipitation method. IOP Conference Series: Materials Science and Engineering. 2020;872(1):012170.
13. Chakraborty KR, Krishna PSR, Chavan SV, Tyagi AK. A neutron diffraction study on ceria-neodia solid solutions. Powder Diffr. 2006;21(1):36-39.
14. Wang F, Richards VN, Shields SP, Buhro WE. Kinetics and Mechanisms of Aggregative Nanocrystal Growth. Chem Mater. 2013;26(1):5-21.
15. Bogush GH, Zukoski CF. Uniform silica particle precipitation: An aggregative growth model. Journal of Colloid and Interface Science. 1991;142(1):19-34.
16. Sukhorukov GB. Controlled Synthesis of Nanoparticles in Microheterogeneous Systems. Von Vincenzo Turco Liveri. Angew Chem. 2006;118(42):7105-7105.
17. Jiang Y, Fu H, Liang Z, Zhang Q, Du Y. Rare earth oxide based electrocatalysts: synthesis, properties and applications. Chem Soc Rev. 2024;53(2):714-763.
18. Titus D, James Jebaseelan Samuel E, Roopan SM. Nanoparticle characterization techniques. Green Synthesis, Characterization and Applications of Nanoparticles:

Elsevier; 2019. p. 303-319.
19. Al-Onazi WA, Ali MHH. Synthesis and characterization of cerium oxide hybrid with chitosan nanoparticles for enhancing the photodegradation of Congo Red dye. Journal of Materials Science: Materials in Electronics. 2021;32(9):12017-12030.
20. Dave M, Dalela S, Kumar S, Alvi PA. Defect induced structural and Raman study of Nd-doped CeO_2 nanomaterials. AIP Conference Proceedings: AIP Publishing; 2020. p. 030108.
21. Raees A, Jamal M, Ahmed I, Silanpaa M, Saad Algarni T. Synthesis and Characterization of CeO_2/CuO Nanocomposites for Photocatalytic Degradation of Methylene Blue in Visible Light. Coatings. 2021;11(3):305.
22. Liu G, Chen X. Chapter 233 Spectroscopic properties of lanthanides in nanomaterials. Handbook on the Physics and Chemistry of Rare Earths: Elsevier; 2007. p. 99-169.
23. Parida KM, Sahu N. Visible light induced photocatalytic activity of rare earth titania nanocomposites. J Mol Catal A: Chem. 2008;287(1-2):151-158.
24. Goldstein JI, Newbury DE, Michael JR, Ritchie NWM, Scott JHJ, Joy DC. Variable Pressure Scanning Electron Microscopy (VPSEM). Scanning Electron Microscopy and X-Ray Microanalysis: Springer New York; 2017. p. 173-185.
25. Handbook of X-Ray Spectrometry. CRC Press; 2001.
26. McBride JR, Hass KC, Poindexter BD, Weber WH. Raman and x-ray studies of $Ce_{1-x}RE_xO_{2-y}$, where RE=La, Pr, Nd, Eu, Gd, and Tb. J Appl Phys. 1994;76(4):2435-2441.
27. Zharkova GM, Osipov VV, Platonov VV, Podkin AV, Strel'tsov SA. Investigation of the Effect of Yttrium Oxide Nanoparticles Doped with Cerium and Neodymium on Electro-Optics of Liquid Crystal Polymer Composites. Russian Physics Journal. 2016;59(8):1295-1301.
28. Courtial P. High-temperature density of lanthanide-bearing Na-silicate melts: Partial molar volumes for Ce_2O_3, Pr_2O_3, Nd_2O_3, Sm_2O_3, Eu_2O_3, Gd_2O_3, Tb_2O_3, Dy_2O_3, Ho_2O_3, Er_2O_3, Tm_2O_3, and Yb_2O_3. Am Mineral. 2005;90(10):1597-1605.
29. Schilling C, Hofmann A, Hess C, Ganduglia-Pirovano MV. Raman Spectra of Polycrystalline CeO_2: A Density Functional Theory Study. The Journal of Physical Chemistry C. 2017;121(38):20834-20849.
30. van Meerloo J, Kaspers GJL, Cloos J. Cell Sensitivity Assays: The MTT Assay. Methods in Molecular Biology: Humana Press; 2011. p. 237-245.
31. Tolosa L, Donato MT, Gómez-Lechón MJ. General Cytotoxicity Assessment by Means of the MTT Assay. Methods in Molecular Biology: Springer New York; 2014. p. 333-348.
32. Dahle JT, Arai Y. Environmental geochemistry of cerium: applications and toxicology of cerium oxide nanoparticles. International journal of environmental research and public health. 2015;12(2):1253-1278.
33. Tuama MJ, Alias MF. Synthesis of ZnO: ZrO_2 Nanocomposites Using Green Method for Medical Applications. Karbala International Journal of Modern Science. 2024;10(3).
34. Buranaamnuay K. The MTT assay application to measure the viability of spermatozoa: A variety of the assay protocols. Open veterinary journal. 2021;11(2):251-269.
35. Hanif A, Ibrahim AH, Ismail S, Al-Rawi SS, Ahmad JN, Hameed M, et al. Cytotoxicity against A549 Human Lung Cancer Cell Line via the Mitochondrial Membrane Potential and Nuclear Condensation Effects of Nepeta paulsenii Briq., a Perennial Herb. Molecules (Basel, Switzerland). 2023;28(6):2812.
36. Nygren P. What is cancer chemotherapy? Acta Oncol. 2001;40(2-3):166-174.
37. Mary Deena D, Prabhu S, Vilwanathan R, Philominal A. Anticancer activity of manganese dioxide/reduced graphene oxide nanocomposites against A549 human lung adenocarcinoma cell line. Nano-Structures & Nano-Objects. 2023;35:101032.
38. Barabas K, Milner R, Lurie D, Adin C. Cisplatin: a review of toxicities and therapeutic applications. Vet Comp Oncol. 2008;6(1):1-18.
39. Perše M. Cisplatin Mouse Models: Treatment, Toxicity and Translatability. Biomedicines. 2021;9(10):1406.
40. Kim JH, Lee K-W, Jung Y, Kim TY, Ham HS, Jong H-S, et al. Cytotoxic effects of pemetrexed in gastric cancer cells. Cancer Sci. 2005;96(6):365-371.
41. Carmichael J, Mitchell JB, DeGraff WG, Gamson J, Gazdar AF, Johnson BE, et al. Chemosensitivity testing of human lung cancer cell lines using the MTT assay. Br J Cancer. 1988;57(6):540-547.
42. Lu VM, Crawshay-Williams F, White B, Elliot A, Hill MA, Townley HE. Cytotoxicity, dose-enhancement and radiosensitization of glioblastoma cells with rare earth nanoparticles. Artificial Cells, Nanomedicine, and Biotechnology. 2019;47(1):132-143.
43. Kumar P, Nagarajan A, Uchil PD. Analysis of Cell Viability by the MTT Assay. Cold Spring Harbor Protocols. 2018;2018(6):pdb.prot095505.